A General Reaction Path Dual-Level Direct Dynamics Calculation of the Reaction of Hydroxyl Radical with Dimethyl Sulfide

S. Sekušak*

Institute Ruđer Bošković, Department of Chemistry, P.O.B. 1016, HR-10001 Zagreb, Republic of Croatia

P. Piecuch

Department of Chemistry, Michigan State University, East Lansing, Michigan 48824

R. J. Bartlett and M. G. Cory

Quantum Theory Project, Departments of Chemistry and Physics, University of Florida, Gainesville, Florida 32611

Received: April 14, 2000; In Final Form: July 19, 2000

Three approaches are used to calculate the gas-phase rate constant for the abstraction of hydrogen by the hydroxyl radical from dimethyl sulfide (i.e., DMS + OH· → DMS· + H_2O): the variational transition state theory approach, a dual-level direct transition state method based on a reaction path determined at the MBPT-(2)/6-31+G(d,p) level, with energetics obtained using the MBPT(2), CCSD, and CCSD(T) methods, and 6-31+G(d,p), 6-311++G(d,p), and 6-311++G(2df,2pd) basis sets. All computed reaction rates include corrections for light atom tunneling. The potential for the dual-level direct dynamics method is supplied by a semiempirical approach in which the PM3 NDDO Hamiltonian has been optimized for this specific class of reactions. The computed thermal rate constants are in good agreement with those determined experimentally, typically within a factor of 2 for our best result. A vibrational-mode correlation analysis is presented. A statistical diabatic model is used to predict changes in the reaction rate due to excitation of a specific vibrational mode in the reactants. A significant enhancement in the rate is predicted for the excitation of the C−H stretching mode.

Introduction

This study investigates the kinetics of the abstraction of hydrogen from dimethyl sulfide (DMS) by the hydroxyl radical (OH·). The reaction

$$\mathrm{DMS} + \mathrm{OH}\cdot \rightarrow \mathrm{DM}\cdot + \mathrm{H_2O} \qquad (1)$$

is a prototype for the general class of hydrogen abstraction reactions of sulfur-containing hydrocarbons. All of these reactions, including the reaction under study, play a key role in combustion processes and in the chemistry of the atmosphere.[1,2] Removal of the OH· radical from the atmosphere by sulfur-containing hydrocarbons, or the lack of removal, is critical to the ongoing discussion of the effect of various compounds released to the atmosphere on the stratospheric ozone layer.

One of our aims is to demonstrate that reasonable estimates of the rate constant characterizing reaction 1 can be obtained if we combine state-of-the-art ab initio methodologies, including many-body perturbation theory[3] (MBPT) and the coupled-cluster (CC) approach,[3a,b,4] with the existing rate theories, including the variational transition state theory (VTST) and its variants.[5] We use an approach in which the MBPT(2) method is first used to determine the minimum energy reaction path (MEP) needed in VTST calculations. The computed energetics of the reaction are then further improved by performing a number of high-level CCSD[6] and CCSD(T)[7] calculations. We also investigate the role of the basis set, including the role of higher polarization functions.

As is the case for every study in which light atoms are being transferred, quantum mechanical tunneling must be taken into account. This is especially true for the hydrogen transfer between DMS and OH·. Furthermore, it is well known that the potential energy surface describing hydrogen atom transfer between two heavy moieties is highly curved,[8] so that accounting for large curvature tunneling[9,10] (LCT) might be an important consideration for reaction 1. To include the multidimensional semiclassical tunneling paths needed for computing the LCT corrections, additional information, apart from the knowledge of the reaction path itself (actually a reaction swath), is required. The problem is that ab initio calculations of the LCT corrections are prohibitively expensive. Thus, a potential energy surface obtained at a lower, less expensive, level of theory is needed for rate constant calculations that include LCT corrections.

In this study, we choose to use the semiempirical Neglect of Diatomic Differential Overlap (NDDO) model Hamiltonian to provide us with the needed reaction swath. An important goal of this study is to develop the model Hamiltonian capable of yielding reliable potential energy surfaces and rate constants for hydrogen abstraction reactions involving OH· and sulfur-containing hydrocarbons. We do it here by reparameterizing the PM3 NDDO Hamiltonian[11] to fundamentally ab initio characteristics of reaction 1, see Table 1. This is the specific reaction parameter (SRP) method[12] of Truhlar et al. Our intent is to develop general reaction parameters[13] (GRP) able to calculate rate constants for a wider category (class) of hydrogen abstraction reactions involving sulfur-containing hydrocarbons

10.1021/jp001417u CCC: $19.00
Published on Web 08/30/2000

TABLE 1: Optimized PM3 Specific Reaction Parameters[a]

parameter	atom	PM3	PM3-SRP	Δ%
U_{ss}	H	−13.073321	−11.739687	10.2
G_{ss}	H	14.794208	15.312414	−3.5
β_s	H	−5.626512	−6.197654	−10.1
U_{ss}	C	−47.270320	−50.762757	−7.4
U_{pp}	C	−36.266918	−37.784164	−4.2
G_{ss}	C	11.200708	10.808798	3.5
G_{sp}	C	10.265027	10.600293	−3.2
G_{pp}	C	10.796292	11.187292	−3.6
G_{p2}	C	9.042566	9.255621	−2.4
H_{sp}	C	2.290980	2.224213	3.1
β_s	C	−11.910015	−12.492375	−4.9
β_p	C	−9.802755	−9.911613	−1.1
U_{ss}	O	−86.993002	−92.961584	−6.9
U_{pp}	O	−71.879580	−69.205865	3.7
G_{ss}	O	15.755760	16.288856	−3.4
G_{sp}	O	10.621160	10.356109	2.6
G_{pp}	O	13.654016	13.042326	4.5
G_{p2}	O	12.406095	12.006452	3.2
H_{sp}	O	0.593883	0.600704	−1.0
β_s	O	−45.202651	−42.892962	5.1
β_p	O	−24.752515	−26.693548	−7.8
U_{ss}	S	−49.895371	−49.235288	1.3
U_{pp}	S	−44.392583	−44.808602	−1.0
G_{ss}	S	8.964667	8.628739	3.7
G_{sp}	S	6.785936	6.691007	1.5
G_{pp}	S	9.968164	9.854839	1.1
G_{p2}	S	7.970247	8.247312	−3.5
H_{sp}	S	4.041836	4.192962	−3.7
β_s	S	−8.827465	−8.426100	4.5
β_p	S	−8.091415	−7.651320	5.4

[a] U, the one-center electron kinetic energy and nuclear attraction in eV; G and H, the two-electron one-center repulsion integrals in eV; β, the resonance integral in eV. Indices correspond to the atomic basis.

and OH·. Reaction 1 gives us an opportunity to test the procedure based on the simpler SRP reparameterized NDDO Hamiltonian.

Rate Theory: Variational-Transition-State Theory

Classical transition-state theory[5] (TST) provides only an upper limit to the exact rate constant due to the "no re-crossing assumption".[5] Varying the location of the hypersurface dividing reactants and products to minimize the computed rate constant (k) yields the variational transition state theory (VTST) rate constant

$$k^{\mathrm{CVT}}(T) = \min_{s} k^{\mathrm{VTST}}(T,s) = (k_{\mathrm{B}}T/h)\kappa(T)\frac{Q^{\ddagger}(T,s_*^{\mathrm{CVT}})}{Q_{\mathrm{r}}} \times \exp[-(\Delta E_0^{\ddagger}(s_*^{\mathrm{CVT}})/RT)] \quad (2)$$

where $\Delta E_0^{\ddagger}(s)$ is the activation energy, s is the reaction coordinate parameter, with s_*^{CVT} being its value at which $k^{\mathrm{VTST}}(T,s)$ reaches its minimum value and $Q^{\ddagger}(T,s_*^{\mathrm{CVT}})$ and Q_{r} are partition functions for the generalized transition state and reactants, respectively. $\kappa(T)$ is the transmission coefficient that accounts for quantum mechanical tunneling. The optimum value of s, s_*^{CVT}, can be obtained by maximizing the generalized free energy, $\Delta G^{\mathrm{GT},0}(T,s)$, and this can be done by calculating energies, gradients, and Hessians along the MEP and interpolating between the calculated points.

Depending upon the nature of the curvature of the MEP, different semiclassical approximations can be used to correct for tunneling. The minimum energy path semiclassical adiabatic ground state (MEPSAG) method is appropriate if the principal tunneling path is along the MEP.[14] This method is also known as the zero-curvature tunneling (ZCT) approach.[13a,b] When the tunneling is assumed to occur on the path defined by the classical turning points on the concave side of the MEP, a centrifugal-dominant small curvature semiclassical adiabatic ground-state (CD-SCSAG) method can be defined.[14b,c] This method is also known as the small-curvature tunneling (SCT) approximation. For light-atom transfer reactions the reaction path can be highly curved, and the large-curvature ground-state approximation, LCT, often becomes the method of choice.[14c,d] The detailed mathematical derivation of, and the resultant formulae for, the ZCT, SCT, and LCT approximations can be found in reference14.

We also explore the effect of the excitation of the reactant vibrational modes on the computed rate constant by using the statistical vibrationally diabatic model.[15] The principal assumption of this model is that vibrational modes preserve their characteristic motions along the reaction coordinate. In this case the vibrational modes can be correlated by maximizing their overlap at successive points along the reaction path. The expression for the vibrational state-selected rate constant differs from the statistical form of the thermal rate expression only in the vibrational partition function for the selected mode. [15]

Computational Details

Electronic Structure Calculations. The geometries of all stationary points along the MEP were optimized and their vibrational frequencies calculated, using second-order many-body perturbation theory, MBPT(2), based on an unrestricted Hartree−Fock[16] (UHF) reference. All optimizations were performed using the 6-31+G(d,p) basis set, and all electrons were correlated. The MBPT(2) energies were obtained using the spin-projected PMP2 scheme.[17] This level of theory is hereafter referred to as level-1. The MEP was determined using the Gonzalez−Schlegel IRC algorithm.[18]

The role of higher order correlation effects was studied by performing the CCSD and CCSD(T) calculations, again including all electrons and employing the UHF reference. Single-point calculations along the MEP obtained with the MBPT(2)/6-31+G(d,p) approach (including reactants, products, and saddle point) using the 6-31+G(d,p) basis set and two larger basis sets, i.e., 6-311++G(d,p) and 6-311++G(2df,2pd), were carried out at these higher levels of theory to obtain more accurate energetics. These additional calculations are referred to as the level-2 calculations. Our best estimate of the energetics was determined by extrapolating the CCSD(T)/6-311++G(d,p) result to the CCSD(T)/6-311++G(2df,2pd) level as follows:

$$E^{\mathrm{CCSD(T)}}[\text{6-311++}G(\text{2df,2pd})] = E^{\mathrm{CCSD(T)}}[\text{6-311++}G(\text{d,p})] + \Delta E^{\mathrm{BS}} \quad (3)$$

where the correction due to the change of basis set, from 6-311++G(d,p) to 6-311++G(2df,2pd), is defined as

$$\Delta E^{\mathrm{BS}} = E^{\mathrm{MBPT(2)}}[\text{6-311++}G(\text{2df,2pd})] - E^{\mathrm{MBPT(2)}}[\text{6-311++}G(\text{d,p})] \quad (4)$$

A similar extrapolation was performed for the CCSD method. We used this extrapolation scheme because it was difficult to perform the CC calculations using the largest, 6-311++G(2df,2pd), basis set. All electronic structure calculations were carried out using the ACESII[19] and the Gaussian 94[20] quantum chemical program packages.

Reaction Rate Calculations. Reaction rate constants are calculated using the interpolated variational transition state

theory with interpolated corrections[21] (IVTST-IC) including ZCT and SCT corrections, and by dual-level dynamics[22] including the LCT correction. The IVTST-IC approach is carried out in two steps. First, we perform the level-1 electronic structure calculations to obtain the energies, gradients, and Hessians for the reactants, products, saddle point and at 40 additional points along the MEP. The energetics are then calculated at the higher levels of theory described above in order to obtain the interpolated corrections to the level-1 energetics. All rate constant calculations are performed using POLYRATE.[23] A three point Lagrangian interpolation is used to calculate the IC energy corrections. The low frequency modes that become imaginary along the reaction path are interpolated directly from the frequencies of the transition state (TS), reactants, and products using the IVTST-0 treatment.[21]

Direct Dynamics Calculations. One of our goals is to develop a semiempirical Hamiltonian that will allow us to calculate rate constants for a variety of hydrogen abstraction reactions, including systems larger than DMS studied here. This can be done using the direct dynamics approach, in which the force field necessary for the rate constant calculation is evaluated on the fly using the semiempirical Hamiltonian. In the direct dynamics method used here we proceed as follows: First, full VTST calculations with optimized multidimensional tunneling are performed using the semiempirical Hamiltonian. Then, the interpolated corrections are used to correct the geometries and vibrational frequencies with respect to those calculated at level-1. The energetics are further improved by using level-2 results.

To obtain the semiempirical Hamiltonian used in direct dynamics calculations, we reparameterize the PM3 variant[24] of the NDDO Hamiltonian by adjusting the one- and two-electron atomic integrals to reproduce, to the extent possible, the energy gradients of the reactants, products, and saddle point obtained at level-1. In addition, we also sought to reproduce the level-2 energetics of the reactants, products, and the saddle point. (We preferentially weighted both the TS structure and the barrier height measured from the reactant side.) The search for the optimum parameter set of the model NDDO Hamiltonian was done stochastically using a genetic algorithm.[25,26] The bounds of the search were limited to ±10% of the initial PM3 parameterization. Due to the similarity of our approach to the specific reaction parameter (SRP) method[12,27,28] of Truhlar et al. We designate the direct dynamics rate constant calculations as SRP calculations.

Results

Experimental Results. The rate constants for the reaction of DMS with the OH· radical, eq 1, have been determined by several experimental techniques. Reaction rate constants for the temperature range of 248 K to 573 K have been reported in reference 29.

Two values for the enthalpy of formation of the DMS radical have been reported in the literature, 32.26 ± 1.20 kcal/mol[30] and 35.6 kcal/mol.[31a] We use the 32.26 ± 1.20 kcal/mol value for the DMS radical together with the experimental heats of formation for DMS −9.0 kcal/mol, for hydroxyl radical 9.4 kcal/mol, and for water −58.0 kcal/mol to obtain an enthalpy of 26.1 kcal/mol for reaction 1. The enthalpy of reaction 1 becomes 22.7 kcal/mol if the second value of the enthalpy of formation (35.6 kcal/mol) is used.[31a]

Stationary Points. Five stationary points were found along the reaction path: reactants, transition state, products, and the van der Waals complexes found on either side of the transition state. The geometries of these points, optimized at level-1, are shown in Figure 1. The optimized transition state structure is reactant-like (an early transition state) with the breaking C_1-H_3 bond being 5% shorter than the forming H_3-O_9 bond. (See Table 2.) This is expected according to the Hammond postulate[32] because the reaction is exothermic.

The van der Waals structures on both the reactant (C_R) and product (C_P) sides of the TS are similar to the unperturbed reactant and product structures. C_R is characterized by the interaction between the sulfur atom and the hydrogen atom of the OH· radical, while the main interaction in the C_P complex is between the carbon radical center and the hydrogen atom of the newly formed water molecule.

The vibrational frequencies were calculated at level-1 to determine the nature of the stationary points. The Hessian computed for the transition-state structure has one negative eigenvalue with an associated eigenvector corresponding to the motion of the hydrogen atom between the C_1 and O_9 atoms. A vibrational analysis was carried out for the van der Waals complexes as well. The three lowest vibrational frequencies of the C_R complex correspond to the normal modes that become the reaction coordinates (Figure 2) for the hydrogen abstraction reactions ($\nu_1 = 33$ cm^{-1} and $\nu_2 = 42$ cm^{-1}) and the decomposition of the complex into reactants ($\nu_3 = 4140$ cm^{-1}). Although two different sets of hydrogen atoms can be distinguished from the symmetry of DMS, only one transition-state structure was found, indicating that the barrier to rotation about the C−S bond is lower than the barrier to abstraction.

Energetics. Barrier heights and reaction enthalpies calculated at the different levels of theory are given in Table 3. Barrier heights calculated at the MBPT(2)/6-311++G(2df,2pd) level and extrapolated CCSD/6-311++G(2df,2pd) level are in good agreement with experiment,[31b] with the CCSD values being somewhat higher in energy than the MBPT(2) values. Inclusion of perturbative T_3 clusters, using the CCSD(T) method, lowers the barrier height by approximately 2 kcal/mol in comparison with the CCSD result. The extrapolation procedure produces CCSD(T) values that are too low in energy, which in turn give the negative barrier heights with the inclusion of the zero-point energy. (See Table 3.) This suggests that the geometries of the saddle point optimized at the MBPT(2) and at the CCSD(T) levels are quite different, although we should verify this statement by performing the TS search at the CCSD(T) level. The same pattern is observed when we compare the results of UHF and MBPT(2) calculations. The geometries of the saddle point calculated at the UHF level differ significantly from those obtained at the MBPT(2) level, and single point MBPT(2) calculations carried out on the UHF structures yield negative barrier heights. Analogous findings were reported for the reaction of the OH· radical with ethane and haloethanes.[33,34] We plan to obtain geometries optimized at the coupled cluster level using the 6-311++G(2df,2pd) basis set.

Reaction Path Properties. The MEP for reaction 1 was computed at level-1 using steps (Δs) of 0.15 a_0 and s values ranging between $s = -3.1331a_0$ and $s = 1.0383a_0$. By convention, the reaction coordinate s is positive on the product side of the saddle point and negative on the reactant side; $s = 0$ defines the saddle point on the Born−Oppenheimer potential energy surface. Figure 3 shows the Born−Oppenheimer potential along the minimum energy path, $V_{MEP}(s)$, the vibrationally adiabatic ground-state potential energy curve, $V_a^G(s)$, and the generalized free energy curve at 298 K, $\Delta G^{GT,0}(s, 298\ K)$. The zero of energy in Figure 3 is defined as the energy of the

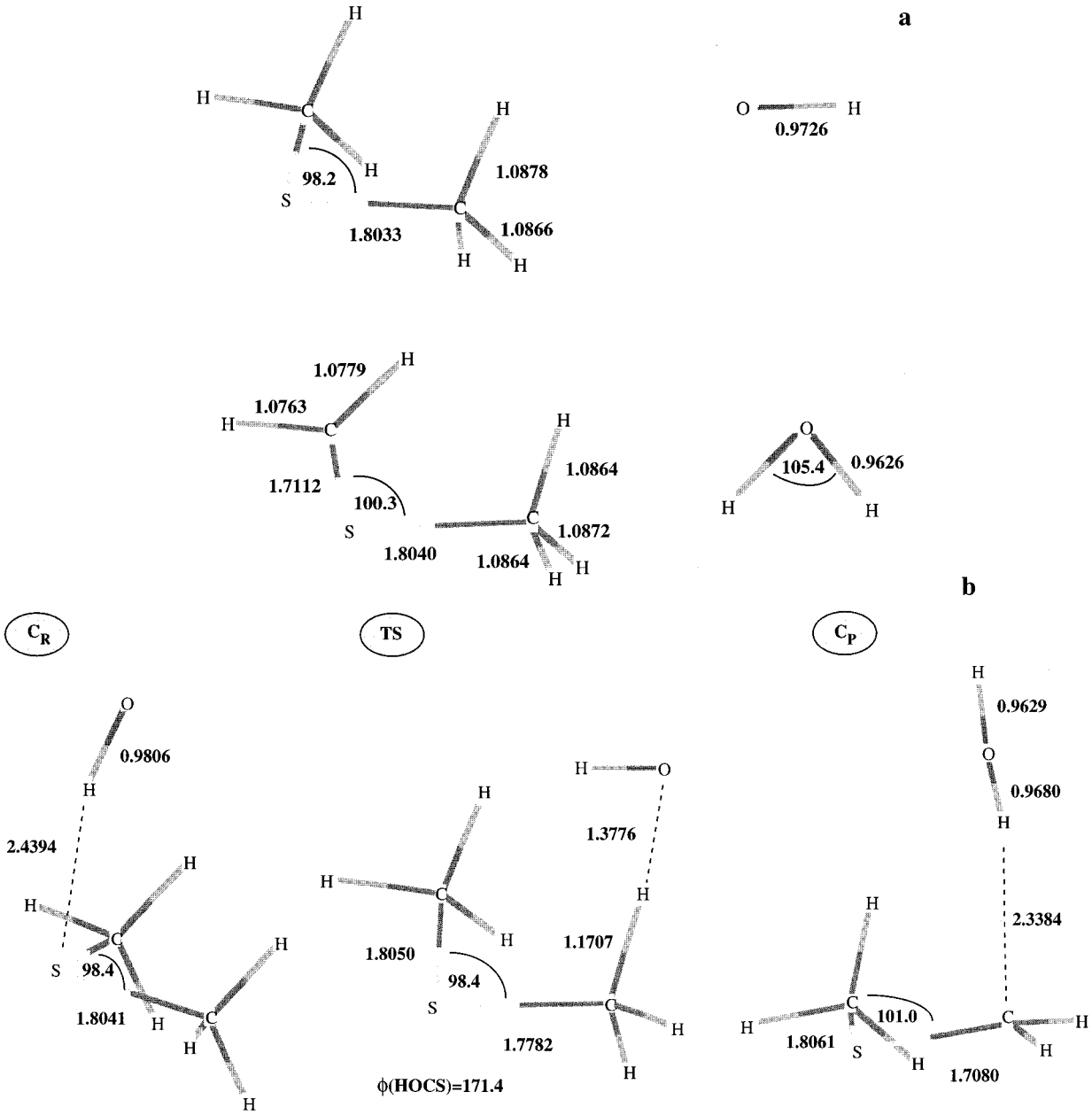

Figure 1. Geometrical parameters for the reactants (a), products (b), transition-state structure (c), and van der Waals complexes (d, e) calculated at the MBPT(2)/6-31+G(d,p) level of theory.

TABLE 2: Geometry, Imaginary Frequency of the Saddle Point, and Energetics of Reaction 1 Obtained with the Standard PM3, Reparameterized Trial PM3-SRP and MBPT(2)/6-31+G(d,p) Methods

	PM3	PM3-SRP	MBPT(2)/ 6-31+G(d,p)
barrier height (kcal/mol)	7.2	2.03	3.1
reaction enthalpy (kcal/mol)	−30.6	−27.7	−23.9
r(C−H) (Å)	1.2378	1.2041	1.3776
r(O−H) (Å)	1.3682	1.3954	1.1707
ϕ(CHO) (degree)	174.3	173.3	171.4
ν_{imsg} (cm^{-1})[a]	2653 i	2251 i	1648 i

[a] Note: The differences in the repulsive curvatures (over the range of 250−400 K) changes the tunneling correction by 10−20%.

reactants. In Table 4 we present the pertinent MEP energetics computed at the MBPT(2) and CCSD(T) levels.

The force constant matrix was also computed every 0.15 a_0 along the MEP, and the generalized normal modes[35] (GNM) were determined. The GNMs were reordered by projecting the eigenvectors of the force constant matrix at successive s values onto one another and by associating those containing the largest contribution from a specific eigenvector to a given GNM. In this way, changes in the frequencies of the GNMs could be followed along the MEP, as shown in Figure 4. Of the 3N-7 GNMs, only those involved in the reaction are shown, and the mode numbering is given with respect to the TS structure. The first GNM, which corresponds to the O−H stretching mode of the reactants, maps to the antisymmetric O−H stretching mode of the product water molecule, and its frequency stays almost constant along the MEP. The ninth GNM, which corresponds to the CH_2 bending mode of the reactant DMS molecule, maps into the symmetric O−H stretching mode of the product water molecule. The 17th GNM, which corresponds to the symmetric CH_3 stretching mode of the reactant DMS molecule, maps to the bending mode of water. The initial direction of the reaction path corresponds to the relative translational motion of the reactants, which maps to the symmetric C−H stretching mode

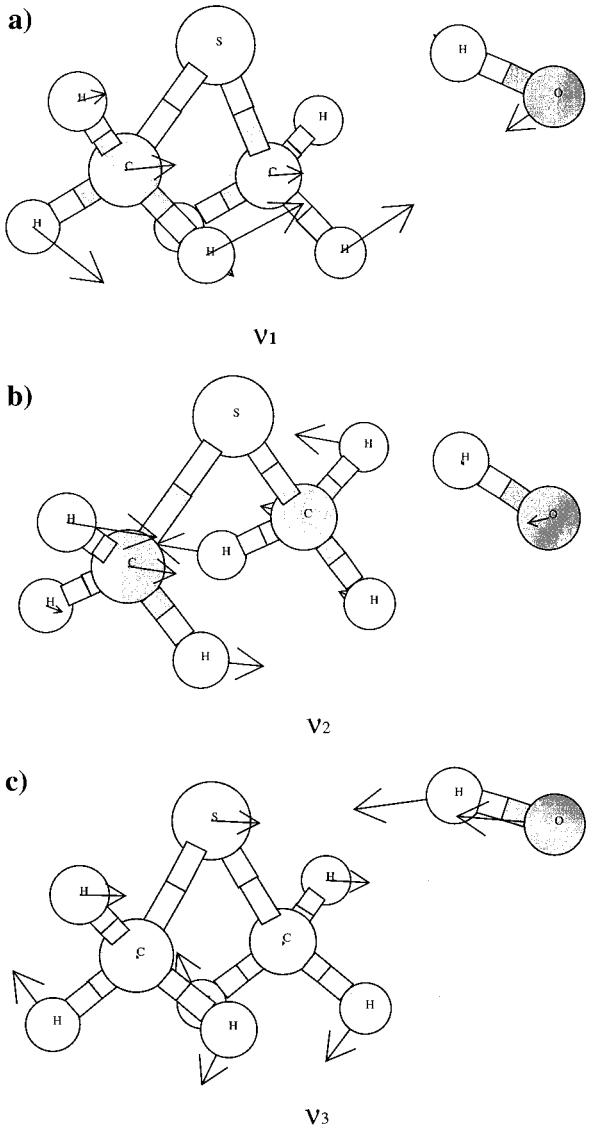

Figure 2. The three lowest vibrational modes for the C_R complex.

TABLE 3: Classical Barrier Height ($\Delta E_o^{\ddagger}$) and the Enthalpy of Reaction 1 ($\Delta_r H^{\phi}$) Calculated at Different Levels of Theory Assuming the Geometries Calculated at the MBPT(2)/6-31+G(d,p) Level[a]

method	$\Delta E_o^{\ddagger}$	$\Delta_r H^{\phi}$
MBPT(2)		
6-31+G(d,p)	4.61 (3.08)	−22.95 (−23.85)
6-311++G(d,p)	7.43 (5.90)	−23.89 (−24.79)
6-311++G(2df,2pd)	2.18 (0.65)	−27.45 (−28.35)
CCSD		
6-31+G(d,p)	5.19 (3.66)	−18.47 (−19.37)
6-311++G(d,p)	7.89 (6.36)	−19.26 (−20.16)
6-311++G(2df,2pd)[b]	2.77 (1.24)	−22.83 (−23.73)
CCSD(T)		
6-31+G(d,p)	2.99 (1.46)	−19.20 (−20.10)
6-311++G(d,p)	5.59 (4.06)	−20.44 (−21.34)
6-311++G(2df,2pd)[b]	0.57 (−0.96)	−24.01 (−24.91)
zero-point energy correction[c]	−1.53	−0.90
experimental value	0.48	−22.68, −25.96

[a] All values are reported in kcal mol^{-1}. Zero-point corrected values of $\Delta E_o^{\ddagger}$ and $\Delta_r H^{\phi}$ are given in parentheses. [b] Extrapolated values as described in the Computational Details section. [c] MBPT(2)/6-31+G(d,p).

at $s \approx -1.0\ a_o$. Further along s, in the direction of the products, this mode becomes the bending mode of the product water molecule. On the product side of the TS, the direction of the s coordinate corresponds to the symmetric stretching mode of water. This mode changes continuously from the bending of the CH_2 group on the reactant side of the TS to the symmetric stretching mode of the water molecule on the product side. For $s > 1.0\ a_o$, the motion along the reaction path is almost purely translational, describing first the formation of the van der Waals complex between product molecules and then the separated product molecules. In the vicinity of the TS, the direction of the reaction path corresponds to the coupling of the C−H and O−H stretching modes, forming the imaginary mode that describes the hydrogen transfer.

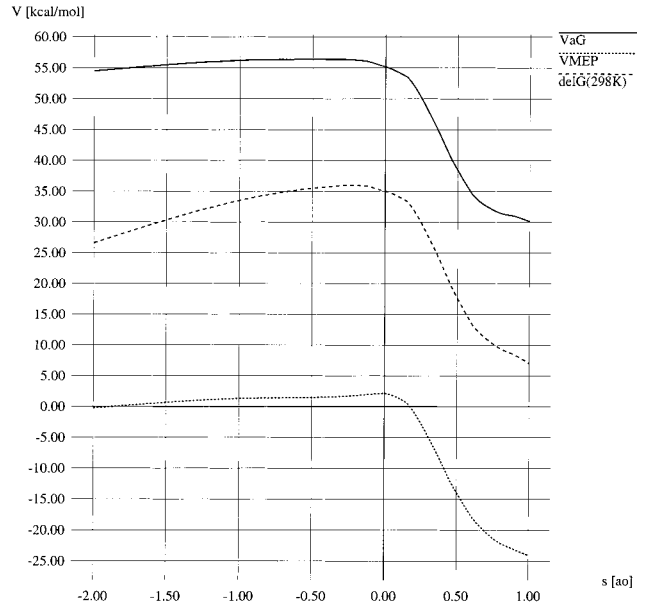

Figure 3. The Born−Oppenheimer potential energy (V_{MEP}), the vibrationally adiabatic ground state potential energy ($V_a^G(s)$), and free energy ($\Delta G^{GT,0}$) at 298 K along the reaction path.

TABLE 4: Energetics[a] along the Minimum Energy Path Calculated at MP2 and CCSD[b] Level of Theory with 6-311++G(2df,2pd) Basis Set for Geometries Calculated at MP2/6-31+G(d,p)[c]

reaction	ΔE_1[d,e]	ΔE_2	ΔE_3	ΔE_4	$\Delta E_o^{\ddagger}$	$\Delta_r H^{\phi}$
MP2/6-311++G(2df,2pd)	−4.12	4.77	−29.37	1.01	0.65	−28.36
CCSD/6-311++G(2df,2pd)	−3.69	4.95	−26.56	2.37	1.24	−23.88

[a] Reactants $\xrightarrow{\Delta E_1}$ Complex-R $\xrightarrow{\Delta E_2}$ TS $\xrightarrow{\Delta E_3}$ Complex-P $\xrightarrow{\Delta E_4}$ Products. [b] Extrapolated as described in the Method section. [c] The barrier heights ($\Delta \mathbf{E}_o^{\ddagger}$) and reaction enthalpies ($\Delta_r \mathbf{H}^{\phi}$) calculated at the same level of theory are shown, as well. All values, corrected for the zero-point energies, are reported in kcal mol^{-1}. [d] $\Delta E = E$(final) − E(initial). [e] Note, spin projection lowers the total second-order energies by between 2 and 3 kcal/mol (depending on the level of theory) and the barriers by between 1.6 and 1.7 kcal/mol.

As can be seen from Figure 4, the GNMs change mostly between $s = -1.0a_0$ to $s = +1.0a_0$. Not surprisingly, the most pronounced changes in the reactive geometric parameters r_{C-H} and r_{O-H} occur in the vicinity of the saddle point. Changes in these distances, as well as the change in the distance between the C and the O atoms, as a function of the position along the MEP, are presented in Figure 5.

The consequences of the above-frequency changes along the MEP for the adiabatic ground-state potential energy are shown in Figure 3. The maximum on the ground-state vibrationally adiabatic potential energy curve $V_a^G(s)$ is shifted to $s_*^{AG} = -0.29a_0$. This shift of the maximum toward the reactants (negative s values) is due to the large change in the frequencies

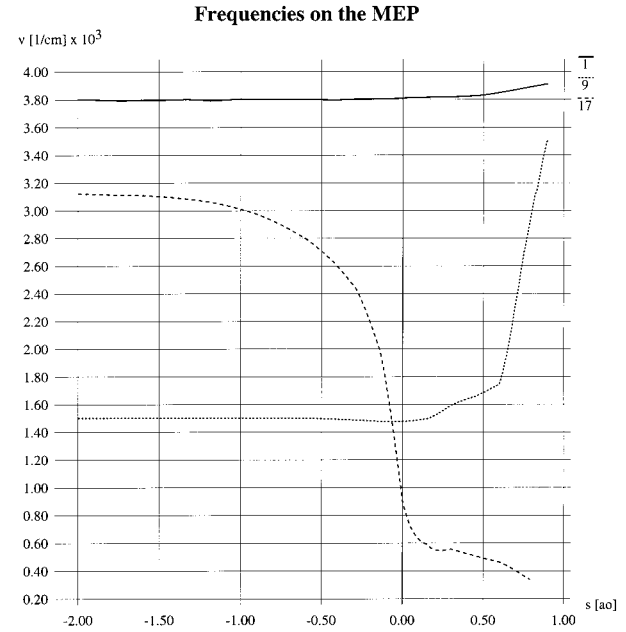

Figure 4. The vibrational-mode correlation analysis for three "reactive" generalized normal modes.

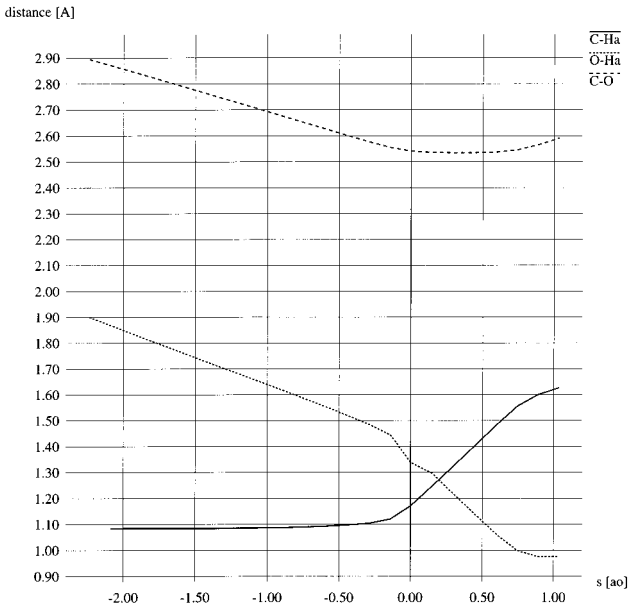

Figure 5. Change of the reactive geometrical parameters r(C−Ha) and r(O−Ha), and of the distance between the C and O atoms along the minimum energy path.

of the CH_2 bending mode on the reactant side of the TS, which cannot be offset by a decrease in the potential energy, because the reaction path is relatively flat in this region. On the product side of the TS the opposite is true: The reaction path is much steeper and the change in the potential energy along the path is larger than is the change in the zero-point energy. The canonical variational dividing surface (corresponding to the maximum of the free energy curve) is located at $s_*^{CVT} = -0.256a_0$ at 298 K. This illustrates the relationship between the Born−Oppenheimer potential energy and the zero-point vibrational energy in determining the location of the variational transition state.

Reaction Rate Constants. Three different approaches were used to estimate the temperature dependence of the rate constant: conventional transition-state theory with the Wigner correction for tunneling (TST/W), interpolated variational transition state theory with interpolated corrections using the small curvature method for the tunneling correction (IVTST-IC/SCT or CVT/SCT for short), and dual-level dynamics including the small and the large curvature tunneling corrections and using the reparameterized NDDO Hamiltonian, SRP/SCT and SRP/LCT, respectively. Although in TST/W and CVT/SCT calculations, we primarily relied on the MBPT(2)/6-311++G-(2df,2pd) results, we also used the extrapolated CCSD/6-311++G(2df,2pd) and nonextrapolated CCSD(T)/6-31+G(d,p) results. (See Table 5.) In Table 5 we distinguish between SRP/LCT-HL and SRP/LCT-LL as follows: LL is the direct SRP result, and HL is the ab initio corrected direct SRP result. In addition to Table 5, we compare the Arrhenius plots of the various rate constant calculations performed in this study in Figure 6.

It is remarkable to observe that the ab initio approaches used in this study produce rate constants which are within a factor of 2−4 compared to experimental data. The reparameterized NDDO method (employing ab initio energies and gradients in searching for optimum parameters) gives excellent results as well.

All calculated rate constants have the correct temperature dependence, and the slopes of log k vs $1/T$ curves shown in Figure 6 are almost identical to the slope of the experimental log k vs $1/T$ curve. For the reported temperature range, $T =$ 250−400 K, the role of tunneling corrections is rather small (at $T = 250$ K the tunneling correction is 1.8, and at $T = 400$ K its value is 1.3). This a consequence of the low energy barrier for reaction 1. The role of tunneling would be somewhat larger at lower temperatures.

The success of the dual-level direct dynamics based on the reparameterized semiempirical Hamiltonian is very promising and will allow us to study other reactions involving molecules larger than DMS, reactions for which it may not be possible to perform accurate ab initio calculations at this point.

A statistical diabatic model was used within the IVTST-IC scheme to investigate the effect of exciting vibrational modes in reactants on the computed rates. (See Table 6.) A small rate enhancement is predicted for the excitation of the O−H stretching mode, while a decrease in the reaction rate is predicted for the excitation of the CH_2 bending mode of DMS. The excitation of the CH_2 stretching mode of DMS is expected to increase the rate by an order of magnitude (see Table 6). These effects can be understood by analyzing the locations of the canonical variational transition states for different excitations of vibrational modes of the reactants.

When the O−H stretching mode is excited to $\nu_1 = 1$, only a small variational shift is found with the adiabatic maximum located at $s = -0.2917a_0$ and the canonical variational transition state is located at $s = -0.2553a_0$ at 298 K. For the excitation of the CH_2 bending mode in DMS to $\nu_9 = 1$, a larger variational shift is found, with the adiabatic maximum positioned at $s = -0.5850a_0$, and the canonical variational transition state is located at $s = -0.2655a_0$ at 298 K. A much larger variational shift is found for the excitation of the CH_2 stretching mode in DMS to $\nu_{17} = 1$. In this case, the adiabatic maximum is positioned at $s = -1.0184a_0$ and the canonical variational transition state is located at $s = -0.5336a_0$ at 298 K.

Summary

The rate constant calculations for the DMS + OH· reaction were performed using high-level electronic structure calculations, interpolated variational transition state theory, dual-level direct dynamics, and multidimensional semiclassical tunneling corrections. Five stationary points were found along the reaction

TABLE 5: Calculated and Experimental Rate Constants[a] for the Reaction of DMS with the OH radical

T (K)	TST/W			CVT/SCT[b]	SRP/SCT-HL	SRP/LCT-HL	SRP/SCT-LL	exp.
276	2.68[b]	1.18[c]	0.61[d]	0.13	1.03	0.88	0.91	4.14
298	2.68[b]	1.25[c]	0.69[d]	0.16	1.09	0.95	0.98	4.26
300	2.69[b]	1.26[c]	0.69[d]	0.17	1.09	0.95	0.99	4.75
359	2.78[b]	1.48[c]	0.89[d]	0.29	1.28	1.16	1.24	5.45
374	2.81[b]	1.53[c]	0.95[d]	0.33	1.34	1.22	1.32	5.71
397	2.88[b]	1.53[c]	1.04[d]	0.39	1.40	1.29	1.45	5.69

[a] k × 10^{12} (cm^3/molecule-sec). [b] The MBPT(2)/6-311++G(2df,2pd) energetics. [c] Extrapolated CCSD/6-311++G(2df,2pd) energies. [d] The CCSD(T)/6-31+G(d,p) result.

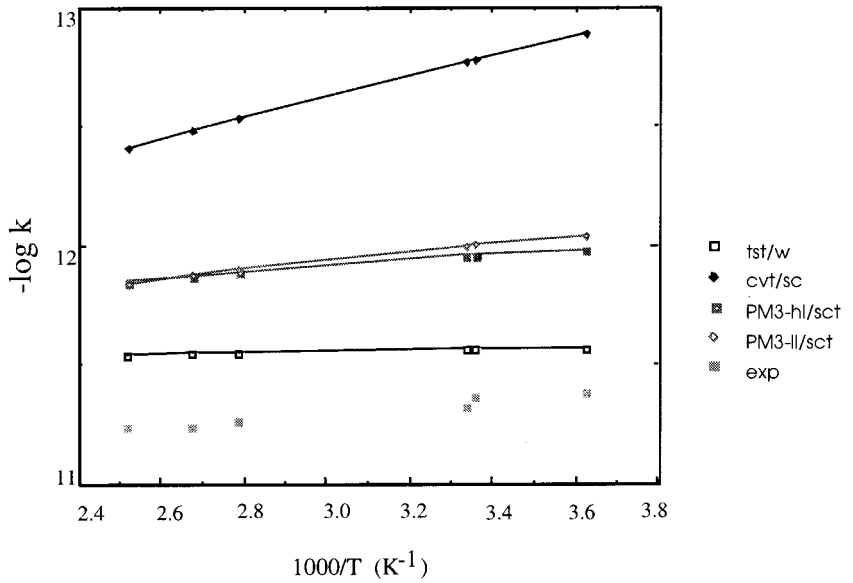

Figure 6. Temperature dependence of the experimental and calculated reaction rate constants.

TABLE 6: Rate Enhancement Factors for the DMS + OH· Reaction Resulting from Excitation of the OH· Stretching (ν_1), CH_2 Bending (ν_9), and CH_2 Stretching (ν_{17}) Modes by One Quantum[a]

T (K)	DMS ($\nu_1 = 1$) + OH	DMS ($\nu_9 = 1$) + OH	DMS ($\nu_{17} = 1$) + OH
276	1.14	0.12	18.54
298	1.12	0.15	16.51
300	1.12	0.15	16.34
359	1.10	0.21	12.32
374	1.10	0.22	11.55
397	1.09	0.25	10.55

[a] Rate constants were obtained using the IVTST-IC approach.

path, including the reactants, the transition state, the products, and the van der Waals complexes formed by the reactants and products. Only one saddle point of first order was found, which can be characterized as an "early" transition state with the breaking C−H bond significantly shorter than the forming O−H bond, and both reactants only slightly deformed compared to their equilibrium geometries.

Good agreement with experimental rate constants was obtained using the MBPT(2)/6-311++G(2df,2pd) and CC data extrapolated to 6-311++G(2df,2pd) basis set from smaller basis set CC calculations. The dual-level direct dynamics based on the reparameterized NDDO Hamiltonian (to reproduce the MBPT(2)/6-31+G(d,p) geometries and gradients of the reactants, products, TS, and the corresponding MBPT(2)/6-311++G(2df,2pd) energies) and VTST turned out to be a very promising approach to accurate rate constant calculations. It is our belief these SRPs will prove to be general in the sense that they are independent of the reaction used to reparameterize the semiempirical Hamiltonian, DMS + OH·; i.e., they are general within the class of reaction for which they were optimized. (In this case, abstraction from sulfur containing hydrocarbons.) This would imply the parametrization obtained in this work could be used in the calculation of rate constants for other hydrogen abstraction reactions for which accurate ab initio calculations may not be possible at this point. (This was the case for the systems we studied in reference 13.) Among other things, this would make possible the study of many important atmospheric reactions that have not yet been studied experimentally or via computational chemistry techniques. We are now testing our rationale.

The large curvature tunneling effect was found to be small, for the temperature range of atmospheric importance, due to the low energy barrier. Finally it was demonstrated that excitation of the CH_2 stretching mode in DMS leads to a large enhancement of the rate of reaction 1.

Acknowledgment. This work was supported by the AFOSR under grant No. F49620-98-0116, and the NSF under grant No. BMR9980015.

References and Notes

(1) Progress and problems in atmospheric chemistry; *Advanced Series in Physical Chemistry*, Barker, J. R., Ed.; World Scientific Publishing Co.: Singapore, 1995; Vol. 3.

(2) Manzer, L. *Science* **1990**, *249*, 31. (b) Solomon, S. *Nature* **1990**, *347*, 6291. (c) Freemantle, M. *Chem. Eng. News* **1994**, *72* (No. 38), 29. (d) Schwarzbach, S. E. *Nature* **1995**, *376*, 297.

(3) Bartlett, R. J. *Annu. Rev. of Phys.* **1981**, *32*, 359. (b) Bartlett, R. J. *J. Phys. Chem.* **1989**, *93*, 1697. (c) Paldus, J.; Čižek, J. *Adv. Quantum Chem.* **1975**, *9*, 105.

(4) Čižek, J. *J. Chem. Phys.* **1966**, *45*, 4256.

(5) Pelzer, H.; Wigner, E. *Z. Phys. Chem. B* **1932**, *15*, 445. (b) Eyring, H. *J. Chem. Phys.* **1935**, *3*, 107. (c) Glasstone, S.; Laidler, K.; Eyring, H.

The Theory of Rate Processes, McGraw-Hill: New York, 1941. (d) Moore, J.; Pearson, R. G. *Kinetics and Mechanism*, 3rd ed., Wiley: New York, 1981.

(6) Purvis, G. D., III; Bartlett, R. J. *J. Chem. Phys.* **1982**, *76*, 1910.

(7) Urban, M.; Noga, J.; Cole, S. J.; Bartlett, R. J. *J. Phys. Chem.* **1985**, *83*, 4041, (b) Raghavachari, K.; Trucks, G. W.; Pople, J. A.; Head-Gordon, M. *Chem. Phys. Lett.* **1989**, *157*, 479.

(8) Tucker, S. C.; Truhlar, D. G. *New Theoretical Concepts for Understanding Organic Reactions*; Bertran, J., Csizmadia I. G., Eds., Kluwer: Dordretch, The Netherlands, 1989; p 291. (b) Kreevoy, M. M., Truhlar, D. G. *Investigation of Rates and Mechanisms of Reactions*, 4th ed., Bernasconi, C. F., Ed.; Wiley: New York, 1986; Vol. 1, p 13. (c) Sekušak, S., Liedl, K. R., Rode, B. M., Sabljić, A. *J. Phys. Chem. A* **1997**, *101*, 4245.

(9) Truhlar, D. G.; Isaacson, A. D.; Garrett, B. C. In *Theory of Chemical Reaction Dynamics*; Baer, M., Ed.; CRC Press: Boca Raton, 1985; Vol. 4, p 65.

(10) Garrett, B. C.; Truhlar, D. J. *J. Am. Chem. Soc.* **1979**, *101*, 4534. (b) Garrett, B. C.; Truhlar, D. J. *J. Am. Chem. Soc.* **1979**, *101*, 5207.

(11) Stewart, J. J. P. *J. Comput. Chem.* **1989**, *10*, 209. (b) Stewart, J. J. P. *Comput.-Aided Mol. Des.* **1990**, *4*, 48. (c) Dewar, M. J.; Thiel, W. *J. Am. Chem. Soc.* **1977**, *99*, 4899, 4907.

(12) Truhlar, D. G. In *The Reaction Path in Chemistry: Current Approaches and Perspectives*; Heidrich, D., Ed.; Kluwer: Dordrecht, 1995; p 229.

(13) Sekušak, S.; Cory, M. G.; Bartlett, R. J.; Sabljiæ, A. *J. Phys. Chem. A* **1999**, *103*, 11394.

(14) Truhlar, D. G.; Kupperman, A. *J. Am. Chem. Soc.* **1971**, *93*, 1840. (b) Truhlar, D. G.; Isaacson, A. D.; Skodje, R. T.; Garrett, B. C. *J. Phys. Chem.* **1982**, *86*, 2252. (c) Skodje, R. T.; Truhlar, D. G.; Garrett, B. C. *J. Phys. Chem.* **1981**, *85*, 3019. (d) Garett, B. C.; Truhlar, D. G.; Wagner, A. F.; Dunning, T. H., Jr. *J. Chem. Phys.* **1983**, *78*, 4400. (e) Bondi, D. K.; Connor, J. N. L.; Garett, B. C.; Truhlar, D. G. *J. Chem. Phys.* **1983**, *78*, 5981.

(15) Truhlar, D. G.; Isaacson, A. D. *J. Chem. Phys.* **1982**, *77*, 3516.

(16) Szabo, A.; Ostlund, N. S. *Modern Quantum. Chem.* McGraw-Hill: New York, 1997.

(17) Schlegel, H. B. *J. Phys. Chem.* **1988**, *92*, 3075.

(18) Gonzalez, C.; Schlegel, H. B. *J. Phys. Chem.* **1990**, *94*, 5523.

(19) Stanton, J. F.; Gauss, J.; Watts, J. D.; Nooijen, M.; Oliphant, N.; Perera, S. A.; Szalay, P. G.; Lauderdale, W. J.; Gwaltney, S.; Beck. S.; Balkova, A.; Bernholdt, D. E.; Baeck, K.-K.; Rozyczko, P.; Sekino, H.; Huber, C.; Bartlett, R. J. ACESII program product of the Quantum Theory Project, University of Florida. Integral packages included are VMOL (Almlof, J. and Taylor, P. R.); VPROPS (Taylor, P. R.); ABACUS (Helgaker, T., Jenson, H. J. Aa., Jorgenson, P., Olsen, J., Taylor, P. R.).

(20) Frisch, A. M. J.; Trucks, G. W.; Head-Gordon, M.; Gill, P. M. W.; Wong, M. W.; Foresman, J. B.; Johnson, G. B.; Schlegel, H. B.; Robb, M. A.; Replogle, E. S.; Gomperts, R.; Anders, J. L.; Raghavachari, K.; Binkley, J. S.; Gonzalez, C.; Martin, R. L.; Fox, D. J.; Defrees, D. J.; Baker, J.; Stewart, J. J. P.; Pople, J. A. *Gaussian92*, Gaussian Inc., Pittsburgh, PA, 1992. (b) Frisch, A. M. J.; Trucks, G. W.; Schlegel, H. B.; Gill, P. M. W.; Johnson, B. G.; Robb, M. A.; Cheesman, J. R.; Keith, T. A.; Petersson, G. A.; Montgomery, J. A.; Raghavachari, K.; Al-Laham, M. A.; Zakrzewski, V. G.; Ortiz, J. V.; Foresman, J. B.; Cioslowski, J.; Stefanov, B. B.; Nanayakkara, A.; Challacombe, M.; Peng, C. Y.; Ayala, P. Y.; Chen, W.; Wong, M. W.; Andres, J. L.; Replogle, E. S.; Gomperts, R.; Martin, R. L.; Fox, D. J.; Binkley, J. S.; Defrees, D. J.; Baker, J.; Stewart, J. P.; Head-Gordon, M.; Gonzalez, C.; Pople, J. A. *Gaussian 94, Revision C.2*. Gaussian, Inc.: Pittsburgh, PA, 1995.

(21) Hu, W.-P.; Liu, Y.-P.; Truhlar, D. G. *J. Chem. Soc., Faraday. Trans.* **1994**, *90*, 1715.

(22) Garrett, B. C.; Truhlar, D. G. *J. Am. Chem. Soc.* **1979**, *101*, 4534, 5207. (b) Truhlar, D. G.; Garrett, B. C. *Annu. Rev. Phys. Chem.* **1984**, *35*, 159. (c) Truhlar, D. G.; Garrett, B. C.; Klippenstein, S. J. *J. Phys. Chem.* **1966**, *100*, 12771. (d) Truhlar, D. G.; Heidrich (ur.), D. *The Reaction Path in Chemistry: Current Approaches and Perspectives*, Kluwer: Dordrecht, 1995, p 229. (e) Truhlar, D. G.; Garrett, B. C. *Acc. Chem. Res.* **1980**, *13*, 440. (f) Truhlar, D. G.; Isaacson, A. D.; Garrett, B. C.; Baer (ur.), M. *Theory of Chemical Reaction Dynamics*, CRC Press: Boca Raton, 1985; Vol. 4, p 65.

(23) Steckler, R.; Hu, W.-P.; Liu, Y.-P.; Lynch, G. C.; Garrett, B. C.; Isaacson, A. D.; Lu, D.-H.; Melissas, V. S.; Truong, T. N.; Rai, S. N.; Hancock, G. C.; Lauderdale, J. G.; Joseph, T.; Truhlar, D. G. *POLYRATE* version 7.8.1, University of Minnesota, Minneapolis, 1998. (b) Lu, D.-h.; Truong, T. N.; Melissas, V. S.; Lynch, G. C.; Liu, Y.-P.; Garrett, B. C.; Steckler, R.; Isaacson, A. D.; Rai, S. N.; Hancock, G. C.; Lauderdale, J. G.; Joseph, T.; Truhlar, D. G. *Comput. Phys. Commun.* **1992**, *71*, 235.

(24) Dewar, M. J. S.; Thiel, W. *J. Am. Chem. Soc.* **1977**, *99*, 4899. (b) Bingham, R. C.; Dewar, M. J. S. *J. Am. Chem. Soc.* **1975**, *97*, 1285. (c) Stewart, J. J. P. *J. Comput. Chem.* **1989**, *10*, 209.

(25) Goldberg, D. E. Genetic Algorithms in search, optimization and machine learning. *Physical Chemistry*; Addison−Wesley: Reading, 1989.

(26) Carroll, D. L. *GaFortran*, version 1.6.4., University of Illinois, 1997.

(27) Page, M. *Comput. Phys. Commun.* **1994**, *84*, 115.

(28) Peslherbe, G. H.; Hase, W. L. *J. Chem. Phys.* **1996**, *104*, 7882.

(29) Atkinson, R. *J. Phys. Chem. Ref. Data*, 1989, Monograph 1.

(30) *CRC Handbook of Chemistry and Physics*, 74th ed.; Lide, D. R., Frederikse, H. P. R., Eds.; CRC Press: Boca Raton, Florida. 1993−1994.

(31) Atkinson, R.; Baulch, D. L.; Cox, R. A.; Hampson, R. F., Jr.; Kerr, J. A.; Troe, J. *J. Phys. Chem. Ref. Data* **1989**, *18*, 881. (b) Martell, J. M.; Mehta, A. K.; Pacey, P. D.; Boyd, R. J. *J. Phys. Chem.* **1995**, *99*, 8661.

(32) Hammond, G. S. *J. Am. Chem. Soc.* **1955**, *77*, 334.

(33) Sekušak, S.; GŸsten, H.; Sabljić, A. *J. Phys. Chem.* **1996**, *100*, 6212; Erratum, **1997**, *101*, 967. (b) Sekušak, S.; GŸsten, H.; Sabljić, A. *J. Chem. Phys.* **1995**, *102*, 7504.

(34) Sekušak, S.; Cory, M. G.; Bartlett, R. J.; Sabljić, A. *J. Phys. Chem. A*, **1999**, *103*, 11394.

(35) Miller, W. H.; Handy, N. C.; Adams, J. E. *J. Chem. Phys.* **1980**, *72*, 99.